Monthly Notices
of the
ROYAL ASTRONOMICAL SOCIETY

MNRASL **430,** L25–L29 (2013) doi:10.1093/mnrasl/sls045

Dark matter chaos in the Solar system

J. Lages[1] and D. L. Shepelyansky[2]⋆

[1]*Institut UTINAM, Observatoire des Sciences de l'Univers THETA, CNRS & Université de Franche-Comté, F-25030 Besançon, France*
[2]*Laboratoire de Physique Théorique du CNRS, IRSAMC, Université de Toulouse, UPS, F-31062 Toulouse, France*

Accepted 2012 November 28. Received 2012 November 27; in original form 2012 November 6

ABSTRACT

We study the capture of Galactic dark matter particles in the Solar system produced by rotation of Jupiter. It is shown that the capture cross-section is much larger than the area of the Jupiter orbit being inversely diverging at small particle energy. We show that the dynamics of captured particles is chaotic and is well described by a simple symplectic dark map. This dark map description allows us to simulate the scattering and dynamics of 10^{14} dark matter particles during the lifetime of the Solar system and to determine the dark matter density profile as a function of distance from the Sun. The mass of captured dark matter in the radius of the Neptune orbit is estimated to be $2 \times 10^{15} g$. The radial density of captured dark matter is found to be approximately constant behind the Jupiter orbit being similar to the density profile found in galaxies.

Key words: chaos – dark matter.

1 INTRODUCTION

A Galactic wind of dark matter particles (DMP; see e.g. Bertone, Hooper & Silk 2005) flies through the Solar system (SS) and a part of it becomes captured due to rotation of planets around the Sun. The capture process, dominated by Jupiter, is related to the non-trivial aspects of the restricted three-body problem (see e.g. Valtonen & Karttunen 2005). We demonstrate that this process is described by a simple dynamical symplectic map (see e.g. Chirikov 1979; Lichtenberg & Lieberman 1992) which allows us to perform extensive numerical simulations of DMP capture. Our studies show that the capture cross-section is much larger than the area of the Jupiter orbit being diverging as an inverse square of DPM velocity in agreement with recent analytical estimates by Khriplovich & Shepelyansky (2009).

The dynamical map analysis allows us to simulate DMP capture and ejection on the whole lifetime scale of the SS for 10^{14} DMP being more efficient than the direct simulations of DPM dynamics by Peter (2009). Our approach provides a DMP density distribution in the SS with other features of dynamics at present time after 4.5 billion years of evolution of the SS. This DMP distribution is similar to those found in galaxies by Rubin, Ford & Thonnard (1980). The dynamics of DMP is shown to be chaotic having certain similarities with a chaotic comet motion in the SS discussed by Petrosky (1986), Chirikov & Vecheslavov (1989), Duncan, Quinn & Tremaine (2005), Dvorak & Kribbel (1990) and Malyshkin & Tremaine (1999).

Following Bertone et al. (2005) we assume that in a vicinity of the SS the velocity distribution of DMP has a Maxwell form $f(v)\,dv = \sqrt{54/\pi} v^2/u^3 \exp(-3v^2/2u^2)\,dv$ with the average module velocity $u \approx 220\,\mathrm{km\,s^{-1}}$. During a scattering of DMP on the Sun its rescaled total energy $w = -2E/m_d v_p^2$ is changed due to planetary rotation. The main contribution is given by Jupiter, as discussed by Chirikov & Vecheslavov (1989), and hence we base our studies on the case of one planet measuring DMP parameters in units of planet radius r_p and velocity v_p taken as unity, DMP mass $m_d = 1$. The studies of comet dynamics by Petrosky (1986), Chirikov & Vecheslavov (1989) and Duncan et al. (2005) in SS with one rotating planet show that it is well described by a symplectic map and thus DMP dynamics over an extended orbit is also described by that type of map.

2 DARK MAP DESCRIPTION

This dark map has a form similar to the Halley map (see Chirikov & Vecheslavov 1989):

$$w_{n+1} = w_n + F(x_n)\,, \quad x_{n+1} = x_n + w_{n+1}^{-3/2}\,, \tag{1}$$

where $x_n = t_n/T_p$ (mod1) is given by time t_n taken at the moment of DMP nth passage through perihelion and T_p is the planet period. The second equation in (1) follows from the Kepler law for the DMP orbital period. The amplitude of kick function $F(x)$ is proportional to the ratio of planet mass m_p to the Sun mass $M_\odot$ ($F \sim m_p/M_\odot$) (see Petrosky 1986; Chirikov & Vecheslavov 1989). Its shape depends on DMP perihelion distance q, inclination angle θ between the planetary plane (x, y) and DMP plane, and perihelion orientation angle φ. However, $F(x)$ is independent of energy w for $1/|w| \gg r_p = 1$. Thus, the dark map describes DMP dynamics for bounded and

⋆E-mail: dima@irsamc.ups-tlse.fr

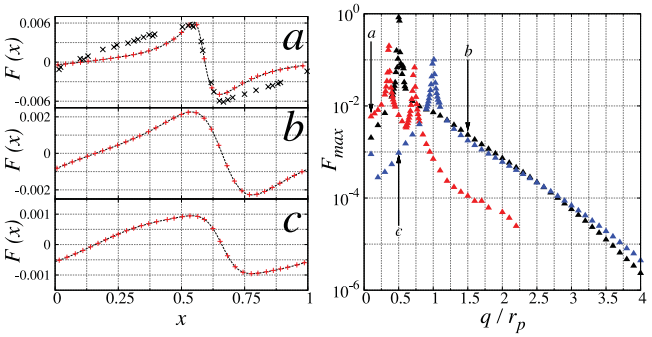

Figure 1. Left-hand panel: dependence of the kick function $F(x)$ on Jupiter phase x for DMP orbit parameters shown by pluses: (*a*) $q = 0.11$, $\theta = 2.83$, $\varphi = 1.95$ of the Halley comet case; here the crosses show data for the Halley comet with all SS planets taken from fig. 1 of Chirikov & Vecheslavov (1989); (*b*) $q = 1.5$, $\theta = 0.7$, $\varphi = \pi/2$; (*c*) $q = 0.5$, $\theta = \pi/2$, $\varphi = 0$; curves show fit functions of numerical data marked by pluses. Right-hand panel: dependence of maximal amplitude $F_{\max}$ on q for a, b, c cases of the left-hand panel.

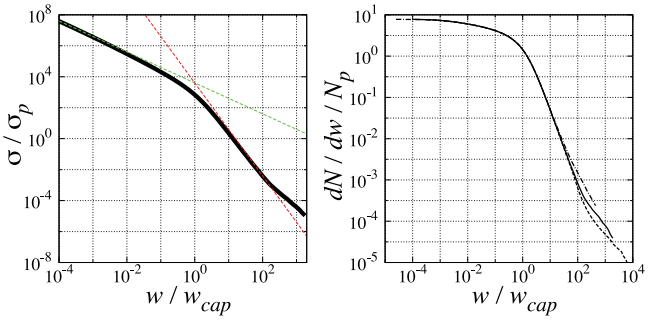

Figure 2. Left-hand panel: dependence of capture cross-section σ for Jupiter on DMP energy w; the dashed lines show dependence $\sigma \propto 1/|w|$; $1/w^2$. Right-hand panel: dependence of rescaled captured number of DMP on energy w for Jupiter, Saturn and a model planet with $m_{\rm p}/{\rm M}_\odot = 0.004$ (full, dashed and dot–dashed curves, respectively).

unbounded energies as well as its capture process corresponding to a transition from positive $w < 0$ to negative energies $w > 0$.

Our direct numerical simulations of Newton equations confirm this map description by the F function as it is shown in Fig. 1 for various values of q, θ, φ, including the Halley comet case analysed by Chirikov & Vecheslavov (1989). In agreement with the theory of Petrosky (1986) the maximum $F_{\max}$ drops exponentially for $q \gg r_{\rm p}$ so that only DMP with $q < 2r_{\rm p}$ can be effectively captured. At $q \gg r_{\rm p}$ we find $F \sim \sin 2\pi x$ in agreement with the results of Petrosky (1986). The visible peaks in $F_{\max}$ correspond to close encounters between DPM and planet happening at rather specific angles for $q \leq r_{\rm p}$. We will see later that such events give a small contribution in the capture cross-section σ. In fact, F function contribution comes from encounter distances of the order of $r_{\rm p}$ thus being much larger than the radius of the planet body $r_{\rm b}$. This analytical result of Petrosky (1986), Chirikov & Vecheslavov (1989), Khriplovich & Shepelyansky (2009) and Shepelyansky (2012) is in agreement with the detailed numerical simulations by Peter (2009) invalidating previous numerical studies of Gould & Alam (2001) and Lundberg & Edsjö (2004) which considered contributions only from $r_{\rm b}$ scale.

Finally, we note that the dark map gives an efficient but approximate description. For the exact dynamics there is a slow variation of DMP orbital momentum ℓ and $q = \ell^2/(2r_{\rm p}v_{\rm p}^2)$ and angles θ, φ (see Dvorak & Kribbel 1990). However, the rate of these variations is rather slow being proportional to $m_{\rm p}/{\rm M}_\odot$ and does not affect significantly the chaotic diffusion in energy. Also numerical simulations of DMP dynamics by Peter (2009) point on a small global variation of q. A similar situation appears in a microwave ionization of Rydberg atoms where it is known that the Kepler map in energy gives a good description of ionization process of 3D atoms as discussed by Shepelyansky (2012). Also the DPM flow $f(v)\,{\rm d}v$ performs an averaging over all ℓ, θ, φ values and hence a variation of these parameters is averaged out.

3 CAPTURE CROSS-SECTION

In a scattering problem at infinity we have $\ell^2 = r_{\rm d}^2 v_{\rm p}^2 |w|$ with the impact scattering distance $r_{\rm d}^2 = 2qr_{\rm p}/|w|$. Hence, the capture cross-section at energy $|w|$ is $\sigma(w)/\sigma_{\rm p} = (\pi^2 r_p |w|)^{-1} \int_0^{2\pi} {\rm d}\theta \int_0^{\pi} {\rm d}\varphi \int_0^{\infty} {\rm d}q h(q, \theta, \varphi)$, where h is a fraction of DMP captured after one map iteration from $w < 0$ to $w > 0$, given by an interval length inside $F(x)$ envelope at $|w| = $ constant, $\sigma_{\rm p} = \pi r_{\rm p}^2$. This fraction is determined from numerically computed $F(x)$, as those shown in Fig. 1, via a continuous fit spline of function $F(x)$. Using a grid with up to $N_{\rm g} = 10^5$ points in (q, θ, φ) volume we perform a Monte Carlo integration which gives $\sigma(w)$ as a function of energy w for the case of Jupiter where the main contribution is given by $|w| \sim w_{\rm cap} = m_{\rm p} v_{\rm p}^2/{\rm M}_\odot \approx 10^{-3}$.

The dependence $\sigma(w)/\sigma_{\rm p}$ is shown in Fig. 2. For $|w| < w_{\rm cap}$ we find $\sigma/\sigma_{\rm p} \approx \pi {\rm M}_\odot w_{\rm cap}/m_{\rm p}|w|$ in agreement with analytical estimates by Khriplovich & Shepelyansky (2009), for $|w| > w_{\rm cap}$ we have $\sigma/\sigma_{\rm p} \approx \pi {\rm M}_\odot w_{\rm cap}^2/(m_{\rm p} w^2)$. The later regime describes contribution of close encounters which has a rapid decrease of σ and hence gives a small contribution in the capture process. This conclusion is confirmed by the analysis of the differential number of captured DMP per time unit ${\rm d}N = \sigma(w) n_{\rm g} v_{\rm p}^2 f(w) {\rm d}|w|/2$. Here $n_{\rm g}$ is a Galactic DMP density with a corresponding mass density $\rho_{\rm g} = m_{\rm d} n_{\rm g} \sim 4 \times 10^{-25}\,{\rm g\,cm^{-3}}$ (see Bertone et al. 2005) and $f(w)$ is the velocity distribution function given above with $|w| = v^2/v_{\rm p}^2$ at infinity. A number of DMP crossing the planet orbit area per time unit is $N_{\rm p} = \int_0^1 n_{\rm g} \sigma_{\rm p} v_{\rm p}^2 f(w)\,{\rm d}|w|/2$.

The dependence of ${\rm d}N/N_{\rm p}{\rm d}w$ on $|w| = v^2/v_{\rm p}^2$, presented in Fig. 2, drops quadratically for $|w| > w_{\rm cap}$ showing that the contribution of close encounters is small. We note that ${\rm d}N/N_{\rm p}\,{\rm d}w$ depends only on the ratio $w/w_{\rm cap}$ that is confirmed by additional data obtained for Saturn and a model planet in Fig. 2. As a result the total number of captured particles is $N \propto m_{\rm p}{\rm M}_\odot$ in agreement with results of Khriplovich & Shepelyansky (2009).

4 CHAOTIC DYNAMICS

To determine the number of captured DMP $N_{\rm cap}(t)$, in SS with Jupiter, as a function of time we model numerically a constant flow of scattered particles with energy distribution ${\rm d}N_{\rm s} \propto vf(v){\rm d}v$ per time unit. The injection, capture, evolution and escape of DMP are described by the dark map (1) with corresponding values of scattered parameters q, θ, φ and corresponding to them $F(x)$ function with the scattering DMP distribution ${\rm d}N_{\rm s} \propto {\rm d}q\,dw$ (we use $q \leq q_{\max} = 4r_{\rm p}$ since above this value $F_{\max}$ is very small).

The scattering and evolution processes are followed during the whole lifetime of SS taken as $t_{\rm S} = 4.5 \times 10^9$ yr. The total number of DMP, injected during time $t_{\rm S}$ in the whole energy range $0 \leq |w| \leq \infty$, is $N_{\rm tot} \approx 1.5 \times 10^{14}$ with $N_{\rm H} = 4 \times 10^9$ scattered DMP in the Halley comet range $0 < |w| \leq w_{\rm H} \approx 0.005$ [$\kappa = N_{\rm tot}/N_{\rm H} \approx 2u^2/(3v_{\rm p}^2 w_{\rm H}) \approx 3.8 \times 10^4$, only DMP with $|w| < F_{\max}$ participate

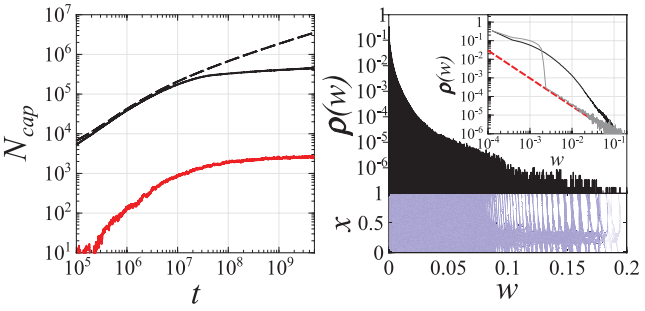

Figure 3. Left-hand panel: the number $N_{\rm cap}$ of captured DMP, as a function of time t in years, for energy range $w > 0$ (dashed curve), $w > 4 \times 10^{-5}$ corresponding to half distance between Sun and Alpha Centauri System (black curve), $w > 1/20$ corresponding to $r < 100$ au (red curve); DMP are injected at constant flow $f(v)$ at all angles. Right-hand panel: the top part shows density distribution $\rho(w) \propto {\rm d}N/{\rm d}w$ in energy at time $t_{\rm S}$ for DMP injection at all parameters q, θ, φ (normalized as $\int_0^\infty \rho\, {\rm d}w = 1$), the bottom part shows the Poincaré section of the dark map for DMP injection at fixed parameters q, θ, φ of Fig. 1(b); the inset shows the density distribution of captured DMP in w in a log–log scale for parameters of Fig. 1(b) (grey curve) and orbits of the main right-hand panel injected at all parameters (black curve), a dashed line shows a slope of $-3/2$.

in dynamics]. We used a random grid of initial q, θ, φ values with up to $N_0 = 4 \times 10^5$ grid points and $N_{\rm i}$ injected orbits at each grid point with $N_{\rm H} = N_0 N_{\rm i}$.

The time dependence $N_{\rm cap}(t)$ in Fig. 3 shows that initially it grows linearly with time. This growth slows down after a time-scale of $t_{\rm d} \approx 10^7$ yr. For a finite SS region with $w > 1/20$ we see that there is a saturation of captured number of DMP. Indeed, according to the results of Chirikov & Vecheslavov (1989) for the Halley comet, the scale $t_{\rm d} \sim 10^7$ yr is a typical scale of diffusive escape of a comet or DMP from SS due to chaotic diffusion in energy. The analytical estimates given by Chirikov & Vecheslavov (1989) and Khriplovich & Shepelyansky (2009) also give a similar escape time. Thus, after that time the injected flow is compensated by the escape process and we obtain a system in an equilibrium state with a fixed number of captured DMP with a certain energy distribution $\rho(w)$.

An example of such a distribution for typical orbit parameters q, θ, φ at present time $t = t_{\rm S}$ is shown in the inset of the right-hand panel of Fig. 3 (grey curve). There is a peak of density at small energies $w < 0.002$ where the orbital period is very long and chaotization is slow. For the range $0.002 < w < w_{\rm ch}$ we have an approximate algebraic decay $\rho \sim 1/w^{3/2}$ which corresponds to the ergodic measure where DMP density is proportional to the orbital period $T_w \sim 1/w^{3/2}$. The chaotic diffusion to large energies is stopped by a critical invariant Kolmogorov–Arnold–Moser curve which separates the chaos region from the integrable one at $w = w_{\rm ch}$.

The analytical estimate of Khriplovich & Shepelyansky (2009), based on the Chirikov criterion (see Chirikov 1979; Lichtenberg & Lieberman 1992), gives for $F_{\rm max} \approx 5 m_{\rm p}/{\rm M}_\odot$ the value $w_{\rm ch} \approx 0.3$ that is in good agreement with the case of Fig. 3 where $w_{\rm ch} \approx 0.2$. In a region $w_{\rm ch}/2 < w < w_{\rm ch}$ we have stability islands, being well visible in the Poincaré section, that gives significant fluctuations in density $\rho(w)$. However, for $w < w_{\rm ch}/2$ the chaos component is homogeneous in the phase plane (w, x). This means that DMP are injected in the chaotic component of a chaotic layer around separatrix $w = 0$, and thus the DMP dynamics in SS is essentially chaotic.

5 DENSITY AND MASS OF CAPTURED DARK MATTER

To obtain DMP space density we consider $N_{\rm tot}$ scattered orbits as described above. Their time evolution is described by the dark map (1) up to the present moment of time $t_{\rm S}$. We keep in memory the initial orbit parameters q, θ, φ of captured orbits. Then we consider only those with $w > 4 \times 10^{-5}$ during the time interval $\delta t_{\rm S}/t_{\rm S} = \pm 10^{-3}$ near time moment $t_{\rm S}$ collecting $\delta N_{\rm AC} \approx 6.2 \times 10^6$ orbits (while instantaneously we have $N_{\rm AC} \approx 3.3 \times 10^5$). For these $\delta N_{\rm AC}$ DMP their dynamics in real space is recomputed from their values of q, θ, φ, w, x during the time period of $\Delta t \approx 100$ Jupiter orbital periods using Newton equations.

The radial density $\rho(r)$ of DMP is obtained by averaging over 10^3 points randomly and homogeneously distributed over this time interval Δt for each of $\delta N_{\rm AC}$ orbits. The obtained normalized radial distribution $\rho(r)$ is shown in Fig. 4 with the corresponding average volume density $\rho_{\rm v} = \rho/r^2$. It corresponds to a stationary equilibrium regime appearing at $t \gg t_{\rm d}$ when injection and escape flows compensate each other. The striking feature of the obtained result is that for $r > r_{\rm p}$ we find $\rho(r) \approx$ constant. This means that the total DMP mass in a radius r grows linearly with r.

According to the virial theorem such a profile gives a velocity of visible matter independent of radius $v_{\rm m}^2 \sim \int_0^r \rho(r')\, {\rm d}r'/r \sim \rho(r)$, being similar to those found in galaxies when the DMP mass is dominant as discussed by Ruben et al. (1980) and Bertone et al. (2005). Another important feature is that the DMP volume density $\rho_{\rm v}$ remains approximately constant for $r < r_{\rm p} = r_{\rm J}$. However, for $r > r_{\rm J}$ this density drops as inverse square distance from the Sun. Thus, we find that a simple model of SS with one rotating planet is able to reproduce significant features of observed DMP density distribution in galaxies.

Let us note that the radial density $\rho(r) \propto {\rm d}N/{\rm d}r$ is only approximately constant for $r > r_{\rm p}$. Indeed, a formal fit of data of Fig. 4 (right-hand panel) in the range $2 < r/r_{\rm p} < 20$ gives $\rho_{\rm v} \sim 1/r^\beta$ with $\beta = 1.53 \pm 0.002$. We can argue that this dependence can be understood from the ergodic measure of effectively one-dimensional chaotic radial dynamics: ${\rm d}\mu \sim {\rm d}N \sim \rho {\rm d}r \sim \int {\rm d}t {\rm d}w ({\rm d}N/{\rm d}w) \sim {\rm d}t \sim {\rm d}r/v_{\rm r} \sim \sqrt{r}\, {\rm d}r$ (assuming that ${\rm d}N/{\rm d}w$ is peaked near $w \approx 0$ as it is seen in the inset of Fig. 3 and hence the radial velocity $v_{\rm r} \sim \sqrt{1/r - w} \sim 1/\sqrt{r}$ and $\rho_{\rm v} \sim 1/r^{3/2}$). Such a dependence would lead to velocity of visible matter $v_{\rm m} \propto \sqrt{\rho} \propto r^{1/4}$ if the DMP mass would be dominant, as it is the case in galaxies as discussed by Ruben et al. (1980).

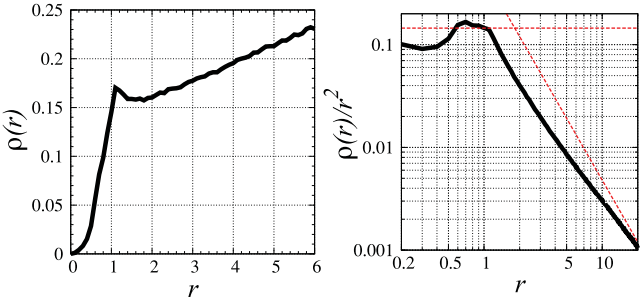

Figure 4. Left-hand panel: radial density $\rho(r) \propto {\rm d}N/{\rm d}r$ at present time $t_{\rm S}$ for SS with Jupiter averaged over all $N_{\rm AC}$ DMP (the normalization is fixed as $\int_0^{6r_{\rm p}} \rho\, {\rm d}r = 1$, $r_{\rm p} = r_{\rm J} = 1$). Right-hand panel: volume density $\rho_{\rm v} = \rho/r^2$ from the data of the left-hand panel, the dashed line shows slope of -2, the horizontal line shows average density for $r_{\rm p}/5 \le r \le r_{\rm p}$.

In fact, the data presented by Ruben et al. (1980, see fig. 7 and equations 1 and 2) are compatible with the dependence $v_m \propto r^{0.35}$ which is close to the above theoretical estimate. However, in SS the DMP mass is small compared to the visible matter and hence the case of galaxies should be analysed in a more detailed way using self-consistent conditions for the DMP distribution which would modify the second equation in the dark map. Though the above arguments can be useful for the analysis of DMP distribution at $r \gg r_p$, in this work we perform the density analysis mainly inside the Neptune orbit where the radial density $\rho(r)$ can be considered as approximately constant.

From the data of Fig. 3 we determine the fraction $\eta_{AC} = N_{AC}/N_{tot} \approx 2.2 \times 10^{-9}$ of DMP captured at time t_S at energies $w > 4 \times 10^{-5}$ and related fraction $\eta_{20} \approx 1.5 \times 10^{-11}$ at energies $w > 1/20$. From Fig. 4 we determine the fraction of N_{AC} orbits in the volume $r \leq 6r_p$ with $\eta_{r6} \approx 4.3 \times 10^{-4}$ and in the volume $r \leq r_p$ with $\eta_{r1} \approx 2.3 \times 10^{-5}$. The DMP mass corresponding to these fractions is obtained by multiplication of these fractions by the total mass of DMP flow passed in the corresponding range $q \leq 4r_p$: $M_{tot} = \int_0^\infty dv v f(v) \sigma \rho_g t_S \approx 69 \rho_g t_S k r_p M_\odot/u \approx 0.9 \times 10^{-6} M_\odot$ where we use the cross-section $\sigma = \pi r_d^2 = 8\pi k M_\odot r_p/v^2$ for injected orbits with $q \leq 4r_p$, k is the gravitational constant ($u/v_p \approx 17$). Thus, the mass of DMP with $w > 4 \times 10^{-5}$ is $M_{AC} \approx \eta_{AC} M_{tot} \approx 2 \times 10^{-15} M_\odot$, and in a similar way the mass at $w > 1/20$ is $M_{20} \approx \eta_{20} M_{tot} \approx 1.3 \times 10^{-17} M_\odot$. The mass M_{AC} can be estimated as a mass of DPM with $|w| < w_H$ absorbed by $F \sim \sin x$ kick during the diffusion time t_d that gives $M_{AC} \sim v_p^2 w_H t_d M_{tot}/(\pi u^2 t_S) \sim 10^{-8} M_{tot} \sim 10^{-14} M_\odot$ being only by a factor of 5 larger than the above numerical value.

The mass of DMP in the volume of the Neptune orbit radius $r < 6r_p$ is $M_{r6} = \eta_{r6} M_{AC} \approx 0.9 \times 10^{-18} M_\odot \approx 1.7 \times 10^{15} g$ and in the radius $r < r_p$ the DMP mass is $M_{r1} = \eta_{r1} M_{AC} \approx 4.6 \times 10^{-20} M_\odot \approx 10^{14} g$. The average volume density of captured DMP inside the Jupiter orbit sphere $r < r_p = r_J$ is $\rho_J = 3M_{r1}/(4\pi r_p^3) \approx 1.2 \times 10^{-4} \rho_g \approx 5 \times 10^{-29}\,\mathrm{g\,cm^{-3}}$. Thus, the density of captured DMP is much smaller than the Galactic DMP density. However, it is by a factor of 4×10^3 larger than the equilibrium DMP Galactic density $\rho_{gH} \approx 0.25 \rho_g/\kappa^{3/2} \approx 1.4 \times 10^{-32}\,\mathrm{g\,cm^{-3}}$ taken in the energy range $0 < |w| < w_H$.

The density distribution of captured DMP in SS is shown in Fig. 5. We see that the density decreases with r at $r > r_J$ in agreement with Fig. 4. A characteristic bulge is formed around the Jupiter orbit. A maximal local volume density is about 10 times larger than the average density ρ_J inside $r < r_J$.

6 DISCUSSION

For further studies it is desirable to take into account the contribution of other planets even if the results presented by Chirikov & Vecheslavov (1989) show that the main features of the dynamics are well described only by Jupiter contribution considered here. It is natural to expect that, as in the SS with one planet, the DMP dynamics in galaxies is dominated by a few stars rotating around the central black hole and thus a constant radial DMP density behind the Jupiter orbit found here should be typical for such galaxies in agreement with observational data discussed by Ruben et al. (1980).

In global our studies show that the average captured DMP density inside the Jupiter orbit is by a factor of 10^4 smaller than the Galactic DMP density ρ_g. The main reason for that is a small value of captured DMP energy $w_{cap} \sim m_p/M_\odot \sim 0.005$ which is very small compared to the dimensional Galactic DMP velocity $u/v_p \sim 17$. However, if we consider the Galactic density in the capture energy range of $0 < |w| < w_{cap}$, then we find that it is significantly enhanced by a factor of 4×10^3 due to the capture process considered here. Thus, the further analysis of chaotic capture process of dark matter in binary systems can bring interesting results.

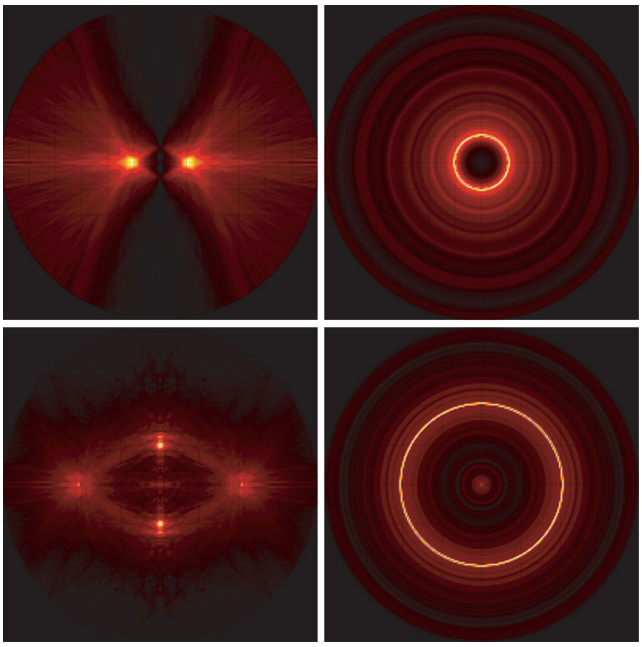

Figure 5. Density of captured DMP in SS at present time t_S. Top panels: DMP surface density $\rho_s \propto dN/dz\, dr_\rho$ shown on *left* in the cross plane $(0, y, z)$ perpendicular to the Jupiter orbit (data are averaged over $r_\rho = \sqrt{x^2 + y^2} =$ constant), on *right* in the Jupiter plane $(x, y, 0)$; only the range $|r| \leq 6r_J$ around the Sun is shown. Bottom panels: corresponding DMP volume density $\rho_v \propto dN/dx\, dy\, dz$ on *left* in the plane $(0, y, z)$, on *right* in the Jupiter plane $(x, y, 0)$; only the range $|r| \leq 2r_J$ around the Sun is shown. Colour is proportional to density with yellow/black for maximum/zero density.

It would be also interesting to consider the inverse ionization process of DMP. According to the dark map (1) the escape velocity square of DMP from a binary system of a star of mass m_s rotating in a vicinity of a black hole of mass M_b is $v_d^2 \sim (m_s/M_b) v_s^2$. For a star moving in a vicinity of the Schwarzschild radius we may have the star velocity $v_s \sim c/3$, and for the mass ratio $m_s/M_b \sim 0.01$ we obtain the escape velocity of DMP $v_d \sim c/30 \approx 10^4\,\mathrm{km\,s^{-1}}$ that is almost hundred times larger than the average Galactic DMP velocity $u \sim 200\,\mathrm{km\,s^{-1}}$. Any other body of mass significantly smaller than m_s is ejected with a similar velocity that can generate compact wandering black holes crossing the Universe at high velocity v_d. Thus, the stars on a distance of the Schwarzschild radius from black holes can work as some kind of black hole accelerators generating high-velocity DMP in the universe.

ACKNOWLEDGMENTS

We thank I. B. Khriplovich for useful discussions. A part of numerical computations has been performed at the mésocentre de calcul de Franche-Comté.

REFERENCES

Bertone G., Hooper D., Silk J., 2005, Phys. Rep., 405, 279
Chirikov B. V., 1979, Phys. Rep., 52, 263
Chirikov B. V., Vecheslavov V. V., 1989, A&A, 221, 146
Duncan M., Quinn T., Tremaine S., 1989, Icarus, 82, 402

Dvorak R., Kribbel J., 1990, A&A, 227, 264
Gould A., Alam S. M. K., 2001, ApJ, 549, 72
Khriplovich I. B., Shepelyansky D. L., 2009, Int. J. Mod. Phys. D, 18, 1903
Lichtenberg A. J., Lieberman M. A., 1992, Regular and Chaotic Dynamics. Springer, Berlin
Lundberg J., Edsjö J., 2004, Phys. Rev. D, 69, 123505
Malyshkin L., Tremaine S., 1999, Icarus, 141, 341
Peter A. H. G., 2009, Phys. Rev. D, 79, 103531
Petrosky T. Y., 1986, Phys. Lett. A, 117, 328
Rubin V. C., Ford W. K., Jr, Thonnard N., 1980, ApJ, 238, 471
Shepelyansky D. L., 2012, Scholarpedia, 7, 9795
Valtonen M., Karttunen H., 2005, The Three-Body Problem. Cambridge Univ. Press, Cambridge

This paper has been typeset from a TEX/LATEX file prepared by the author.